A Magneto-Structural Analysis of Fe(III) Keggin Polyoxometalates.

Nuno A. G. Bandeira,[a,b,c]* Omid Sadeghi,[d] Toby J. Woods,[e] Yuan-Zhu Zhang,[e] Jürgen Schnack,[f]*

Kim Dunbar,[e] May Nyman,[d] and Carles Bo [a,e].

a. Theoretical and Computational Chemistry Laboratory - Institute of Chemical Research of Catalonia (ICIQ), The Barcelona Institute of Science and Technology, 16 Av. Països Catalans, 43007 Tarragona, Spain, Av. Països Catalans 16, Tarragona 43007 Spain.

b. Centro de Química e Bioquímica, Faculdade de Ciências, Universidade de Lisboa, Campo Grande, 1749-016 Lisboa, Portugal.

c. Centro de Química Estrutural, Instituto Superior Técnico, Universidade de Lisboa, Avenida Rovisco Pais, 1049-001 Lisboa, Portugal.

d. Department of Chemistry, Oregon State University, Corvallis, OR 97331, USA.

e. Chemistry Dept. Texas A&M University,P.O. Box 30012,College Station, TX 77842-3012, USA.

f. Fakultät für Physik, Universität Bielefeld, Postfach 100131, D-33501 Bielefeld, Germany.

g. Departament de Química-Física i Inorgànica, Universitat Rovira i Virgili, Carrer Marcel·lí Domingo, Tarragona 43007, Spain.

ABSTRACT

A computational study and magnetic susceptibility measurements of three homonuclear Fe(III) Keggin structures are herein presented: the $[FeO_4@Fe_{12}F_{24}(\mu\text{-}OCH_3)_{12}]^{5-}$ anion (**1**), the $[Bi_6\{FeO_4@Fe_{12}O_{12}(OH)_{12}\}(\mu\text{-}O_2CCCl_3)_{12}]^+$ cation (**2**) and its polymorph $[Bi_6\{FeO_4@Fe_{12}O_{12}(OH)_{10}(H_2O)_2\}(\mu\text{-}O_2CCF_3)_{10}]^{3+}$ (**3**). These results are contrasted with the exchange interactions present in the previously characterised $[Fe_6(OH)_3Ge_2W_{18}O_{68}(OH)_6]^{11-}$ and $[H_{12}As_4Fe_8W_{30}O_{120}(H_2O)_2]^{4-}$ anions. The computational analysis shows that the most significant anti-ferromagnetic spin coupling takes place at the junction between each of the $\{Fe_3O_6(OH)_3\}/\{Fe_3F_6(OCH_3)_3\}$ framework motifs, a possibility that had been previously discarded in the literature on the basis of the Fe-Fe distances. For all the examined iron(III) Keggin structures, it is found that the magnitude of the magnetic couplings within each structural sub-unit follows the same trend.

Introduction

Within the realm of molecular metal oxides, the Keggin[1] structure is by far the most ubiquitous. This archetypal structure consists of a tetrahedral XO_4 unit surrounded by four trimeric edges sharing octahedral $\{M_3O_6(\mu\text{-}O)_3\}$ motifs. The Keggin ion is recognized in many synthetic and natural materials including polyoxocations,[2] polyoxometalates[1] (POMs), ferrihydrite, magnetite and zunyite.[3] Discrete magnetic[4] clusters and nanoclusters (magnetite in particular) respectively have enormous potential as spintronic-based molecular devices for memory storage.[5] The interpretation of susceptibility data of these discrete magnetic clusters is extremely challenging due to their high nuclearity,[6] and the number of valence electrons per metallic unit.[5a]

Considerable advances have been made in the field of magnetic polyoxometalates in particular those containing iron as addenda atoms. Some of these structures incorporate magnetic centres as addenda to lacunary framework structures (e.g. $[M^{III}(SiW_{11}O_{39})_2]^{13-}$), whereas others are built from incorporating dynamic library building blocks such as $\{Fe_{30}Mo_{72}\}$.[5c,7]

Several mixed addenda Keggin structures have been characterised with the general aim of creating new magnetic materials. The works of Xue,[8] Hill,[9] Yang,[10] Niu,[11] Nadjo[12] and others have brought considerable advances to the field. The latter two papers are of interest since they assign magnetic exchange coupling constants to these complexes from magnetic susceptibility measurements. Keggin structures with Fe addenda tend to polymerise to compensate for the inability of iron to achieve a double bond with an oxo ligand, a phenomenon dubbed the 'metal-oxo wall'.[13] These anions are formulated $[H_{12}As_4Fe_8W_{30}O_{120}(H_2O)_2]^{4-}$ (hereinafter $\{As_4Fe_8W_{30}\}$) and $[Fe_6(OH)_3Ge_2W_{18}O_{68}(OH)_6]^{11-}$ ($\{Ge_2Fe_6W_{18}\}$) respectively[11,12] and are depicted in **Figure**

1. The first one is an S shaped molecule that has two triangular {Fe$_3$} motifs on both termini sandwiching a lacunary framework with an {Fe$_2$} oxo dimer. The lacunae are crowned by protonated enH$_2{}^{2+}$ counter-cations. The {Fe$_3$} magnetically active moieties are each anti-ferromagnetically coupled with a J = -14 cm^{-1} while the {Fe$_2$} dimer cluster has negligible antiferromagnetic (AF) interaction (J'=-0.45 cm^{-1}), effectively paramagnetic. The second structure is simpler and consists of two hydroxo bridged {GeFe$_3$W$_9$} monomers. The {Ge$_2$Fe$_6$W$_{18}$} structure may be envisaged as a magnetic trigonal prism with one type of coupling between each side of the equilateral triangle (J) and another one along the sides of the prism axis (J'). The authors assumed J=J' as an approximation in their estimation of J (-24 cm^{-1}).
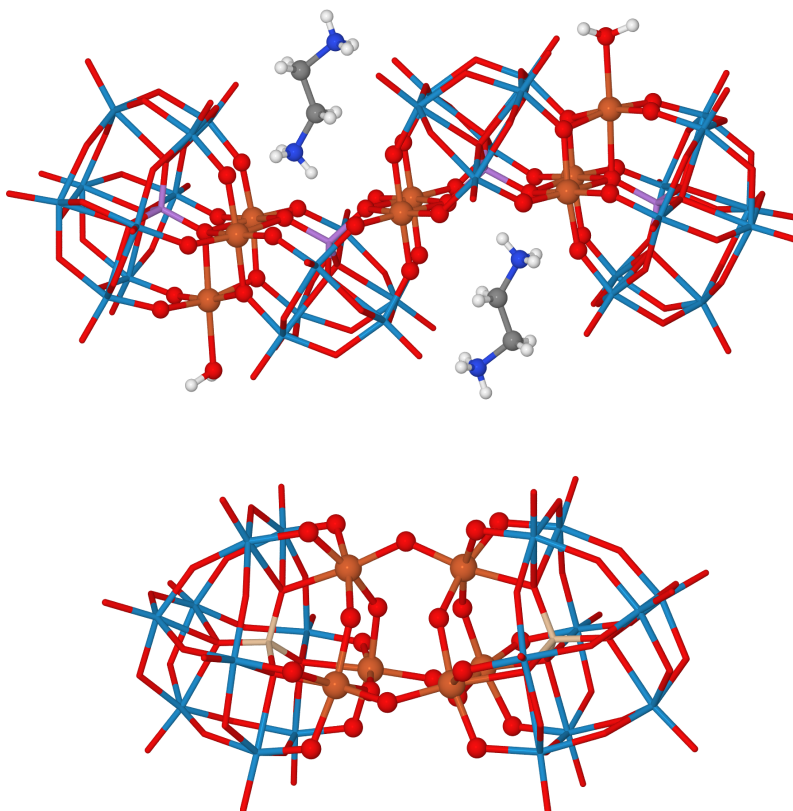

Figure 1 – Two Keggin derivatives {As$_4$Fe$_8$W$_{30}$} (top from ref. [11]) and {Ge$_2$Fe$_6$W$_{18}$} (bottom from ref. [12]) emphasizing the Fe(III) hetero-atom addenda in orange.

Far fewer homo-nuclear polyoxometalates with magnetic properties have been identified, the most notable of which are mixed-valence V(IV)/V(V) poly-anions of varying nuclearity (e.g. {V_{15}},{V_{19}}).[5a] The degree of control of the V(IV)/V(V) ratio can be limited however. The {V_{15}} system in particular has received significant attention. On the theoretical side we have gained greater insight into these clusters with the aid of Density Functional[14] (DFT) and wavefunction methods (DDCI).[15] Further insight has been gained from experiment in the last decade with the works of Tsukerblat[16] and Martens[17] in relation to the pseudo-Jahn-Teller instability and the role that it plays in spin frustration of these orbitally degenerate systems and in their magnetic anisotropy.

A Keggin ion with Fe(III) in both the tetrahedral and octahedral positions {Fe_{13}} has been obtained from both organic solution[18] and water;[19] the latter being of particular interest in understanding the role of pre-nucleation clusters in growth of iron oxyhydroxide materials from water.[20] There is substantial evidence that iron oxides do indeed grow from aggregation of 1 nm discrete clusters. [19-21] The trimer building blocks, referred to as 'triads' and their relative orientation determine the symmetry and type of rotational isomers of this class of compounds. [22] A major hallmark in the quest for Fe^{III} homo-nuclear Keggin structures was the synthesis of the [$FeO_4@Fe_{12}F_{24}(\mu\text{-}OCH_3)_{12}$]$^{5-}$ anion (**1**) by Bino *et al*. [18] (**Figure 3**) in organic solvent. Low valent metal Keggin structures are generally difficult to obtain because they cannot support M=O double bonds nor can they contain μ-oxo bridges due to the excessive negative charge it would entail.

The electronic structure of Fe(III) Keggin structures should consist of linear combinations of weak octahedral ligand field splitting $3d$ orbitals (t_{2g}^{3} e_g^{*2}) with its tetrahedral core (e^2 t_2^{3}), and

the resulting ground state of the Keggin should lie in the spin (de)coupling of these thirteen centres. From symmetry considerations, four triads should have the same magnetic interactions with each neighbour (J_{1b}) as well as within each unit (J_{1a}, **Figure 2**). The same spin coupling (J_2) should come into effect between the twelve iron centres in the outer shell and the tetrahedral core.

The magnetic properties of **1** were subsequently reported.[23] To simplify their analysis, the authors neglected inter-triad exchange couplings justified by the ionicity of the Fe-F bonds, the known predominance of super-exchange in μ-oxo ligands, and the distance between the iron nuclei in each triad junction of 3.8 Å as compared to the intra-triad distances of 3.1 Å. A sketch of the magnetic coupling is shown in **Scheme 1**. The outer layer is made up of triangular motifs originating from the four triads (dark plain lines, J_{1a}), linked by another four different triangular motifs which constitute the inter-triad boundary region (red dashed lines). From their measurements, a two J model Hamiltonian was applied, one reflecting the coupling between the tetrahedral iron centre (Fe_{tet}) and the twelve remaining iron octahedral moieties (Fe_{oct}) valued at J_2 = -43 cm^{-1} and another held constant J_{1a} = -30 cm^{-1}, reflecting AF coupling between the octahedral iron centres within each {Fe_3} triad.
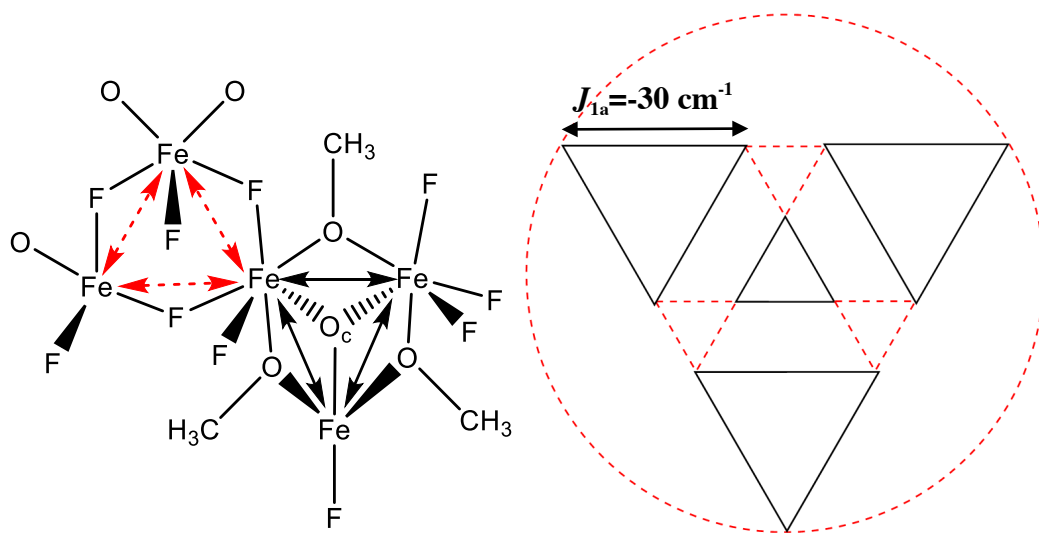
Scheme 1 - Principal chemical unit of the outer shell in 1 (left) and flat sketch of the intra-triad (J_{1a}) magnetic coupling in the shell structure of compound 1 (right, from ref. [23a]). Dashed red lines represent the neglected pathways and O_c denotes a central oxygen belonging to the core {$Fe_{tet}O_4$} sub-unit.
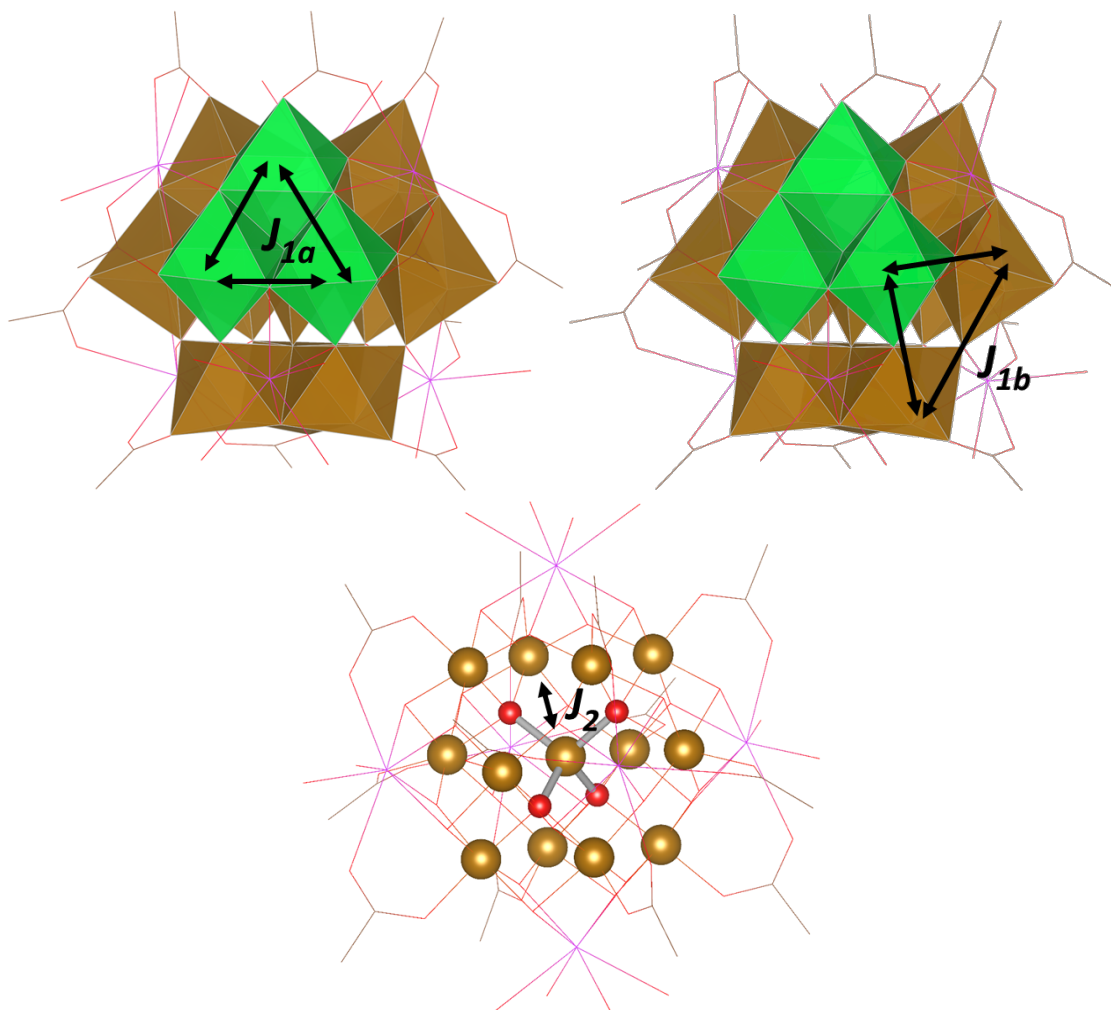
Figure 2 - Nearest neighbor exchange pathways in a Keggin ion (exemplified here as cation **2**): Outer shell to centre (J_2), intra-triad (J_{1a}) and inter-triad (J_{1b}). The triad motif is highlighted in green.
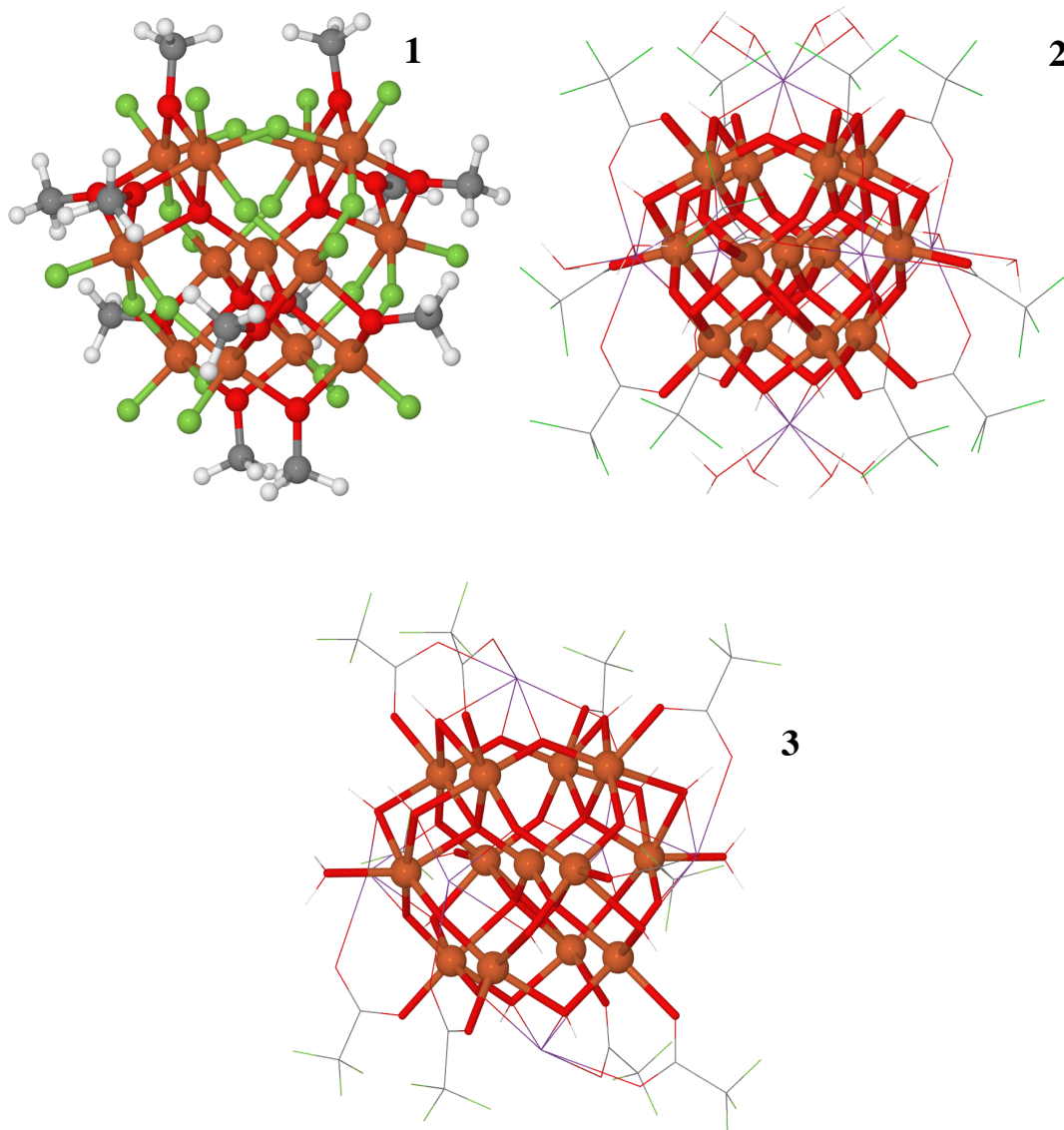
Figure 3 – Crystal structure geometry of three homonuclear Keggin ions: **1,2** and **3**. Hydrogen positions were pre-optimized. The presence of bismuth cations, tri-chloroacetate groups in **2** and tri-fluoroacetates (respectively TCA and TFA) in **3** are represented as a wireframe for clarity. Color codes: Fe rust orange, O red, C grey, H white, Bi purple and halogens are green.

The first all Fe^{III} Keggin structure[19] from water was recently identified as $[Bi_6\{FeO_4@Fe_{12}O_{12}(OH)_{12}\}(\mu\text{-}O_2CCCl_3)_{12}]^+$ (**2**), captured in this discrete state from water by

utilizing Bi^{3+} cations to help stabilise the excessive negative charge which may also act as a templating agent for the whole structure.

A new structural isomer of **2** has recently been characterized by some of us,[24] in which TFA ligands are used to fill the coordination sphere of the $\{Fe_{13}\}$ Keggin instead of the TCA ligands present in **2**. It is fully formulated as $(Na_4)[Bi_6\{FeO_4Fe_{12}O_{12}(OH)_{12}(H_2O)_2\}(\mu\text{-}O_2CCF_3)_{10}](CF_3COO)_5 \bullet xH_2O$ (**3**). Since hydrogen atoms are very difficult to locate, the μ-hydroxo groups were inferred from bond valence sum and bond angle considerations (**Figure 3**). The coordinates of these hydrogen atoms were optimised while keeping the crystal structure coordinates intact. As described previously,[24] each μ^2 bridging site is disordered with 50% occupancy of OH and O so the most symmetric selection was made.

Since there is still no clear understanding of the relationship between each of the structural sub-units in Fe Keggin structures this work aims to shed light on the magneto-structural relationships existing within the motifs of the Keggin architecture. We begin with the heteronuclear Fe species, and then address the homonuclear clusters, in particular to determine how the spin couplings vary inside the triads, inter-triads and tetrahedral core. These efforts will provide guidance to experimentalists in determining correct assignments of the J coupling constants to their respective magnetic motifs. The notable advantage of polyoxometalates as a scaffold for magnetic moieties is that their structural features are fixed (bonds and angles) thus providing sub-unit building blocks to be used as a magnetic "lego kit" in the design of magnetic materials, if control of substitutional positions is achieved. Towards this goal, we will present the structural relationship between the $\{Fe_3\}$ triad in $\{As_4Fe_8W_{30}\}$ the inter-triad dimer in $\{Ge_2Fe_6W_{18}\}$ and the homo-nuclear $\{Fe_{13}\}$ Keggin species previously described.

Additionally we establish the similarities and differences between the three {Fe$_{13}$} Keggin derivatives. To our knowledge this is the first computational investigation of magnetically active Fe(III) homo-nuclear polyoxometalate structures of the Keggin type that aims at a deeper understanding of the experimentally measured magnetic parameters.

Computational Details

The Amsterdam Density Functional (ADF) program package[25] version 2013.01 has been used with Becke's[26] three parameter gradient corrected exchange and Lee, Yang and Parr's correlation[27] functionals (B3LYP) were used in the calculations. The ZORA[28] scalar relativistic Hamiltonian was employed with triple zeta Slater type orbitals[29] (STO) augmented with one polarization function (TZP) for bismuth and iron, and double zeta STO type functions augmented with d functions (DZP) on the remaining elements. The broken symmetry technique of Noodleman and co-workers[30] was used with the non-spin projected formula of Ruiz[31] to take full advantage of the self-interaction error present in the quantitative evaluation of the J constant with standard density functionals.[32] This formula has been generalised by Bencini[33] for polynuclear clusters as

$$\Delta E(S - S_{max}) = \sum_{1<j} J_{ij}(2s_i s_j + s_j) \qquad (1)$$

where s_i and s_j are local spin moments that must be paired. For instance in the case in which Fe$_{tet}$ has an m$_s$=-5/2 and the remaining 12×Fe$_{oct}$ with m$_s$=+5/2 each (S=55/2) the obtained energy difference will be $\Delta E = 12 \times (25/2 + 5/2)J_2 = 180J_2$ since all the terms in the sum are equal. For each

class of J's the values can be obtained from the above formula in accordance with the topologies of the spin flip.

A Heisenberg-Dirac-Van Vleck Hamiltonian of the form

$$\hat{H} = -J_{1a}(\vec{s}_1 \times \vec{s}_2 + \vec{s}_2 \times \vec{s}_3 + \vec{s}_3 \times \vec{s}_1)$$
$$-J_{1a}(\vec{s}_4 \times \vec{s}_5 + \vec{s}_5 \times \vec{s}_6 + \vec{s}_6 \times \vec{s}_4)$$
$$-J_{1a}(\vec{s}_7 \times \vec{s}_8 + \vec{s}_8 \times \vec{s}_9 + \vec{s}_9 \times \vec{s}_7)$$
$$-J_{1a}(\vec{s}_{10} \times \vec{s}_{11} + \vec{s}_{11} \times \vec{s}_{12} + \vec{s}_{12} \times \vec{s}_{10})$$
$$-J_{1b}(\vec{s}_1 \times \vec{s}_7 + \vec{s}_1 \times \vec{s}_{10} + \vec{s}_2 \times \vec{s}_5 + \vec{s}_2 \times \vec{s}_9)$$
$$-J_{1b}(\vec{s}_3 \times \vec{s}_6 + \vec{s}_3 \times \vec{s}_{12} + \vec{s}_4 \times \vec{s}_8 + \vec{s}_4 \times \vec{s}_{11})$$
$$-J_{1b}(\vec{s}_5 \times \vec{s}_9 + \vec{s}_6 \times \vec{s}_{12} + \vec{s}_7 \times \vec{s}_{10} + \vec{s}_8 \times \vec{s}_{11}) \qquad (2)$$
$$-J_2 \vec{s}_{13} \times \sum_{i=1,12} \vec{s}_i)$$
$$+g\mu_B B \sum_{i=1,13} \vec{s}_i$$

was used with standard conventions for the J values (antiferromagnetic $J<0$, ferromagnetic $J>0$). The geometries of the crystal structures were directly used in the calculation. For cations **2** and **3** the hydrogen atoms were previously positioned and pre-optimised with the BP86 GGA class functional before the broken symmetry runs. All negatively charged ions were calculated with the COSMO implicit solvation[34] scheme to circumvent the problem of Kohn-Sham orbital positive energies.

A single point calculation to compute corresponding orbital overlaps was performed using the ORCA[35] program package. An Ahlrichs[36] type split-valence Gaussian type pseudopotential (for Bi only) and basis set augmented with a polarisation function (SVP) were used with the RIJCOSX integral fitting technique[37] while keeping the same functional (B3LYP).

Experimental Details

The iron Keggin ions **2** and **3** were synthesized as prior reported.[19, 24] Since they form large crystals of a distinctive shape and color, inspection is the first step to confirm the product. The purity of samples for magnetic measurement was ascertained by 1) visual inspection of the crystals, 2) unit cell check by single crystal X-ray diffraction, and 3) SAXS. Magnetic susceptibility and magnetization measurements were collected using a Quantum Design MPMS-XL SQUID magnetometer.

Synthesis of $[Bi_6\{FeO_4@Fe_{12}O_{12}(OH)_{12}\}(\mu\text{-}O_2CCCl_3)_{12}]\ O_2CCCl_3.14H_2O$ (2)

The cluster was synthesized as described prior.[19] $Bi(NO_3)_3 \cdot 5H_2O$ (3.88 g, 8 mmol) and $Fe(NO_3)_3 \cdot 9H_2O$ (6.46 g, 16 mmol) was suspended in 15 mL of water and heated to boiling for 15 minutes which led to the formation of a clear red solution. This solution was then added to a boiling solution of 7.84 g (48 mmol) of trichloroacetic acid and 4.12 g (49 mmols) of $NaHCO_3$ in 20 of mL water to form a brown precipitate. The precipitate was dissolved in 20 mL of THF at room temperature. After 24 h of stirring at room temperature, the organic phase was extracted using a separatory funnel and red needles were obtained by slow evaporation. The SQUID sample was prepared by using crushed crystals immobilized in eicosane and sealed in a NMR tube. Sample: 33.97 mg; Eicosane, 50.88 mg; Pascal's constant for eicosane: 282.55 x 10^{-6} emu/mol.

Synthesis of $(Na_4)[Bi_6FeO_4Fe_{12}O_{12}(OH)_{12}(H_2O)_2(CF_3COO)_{10}](CF_3COO)_4.(CO_3)_{1.5}.16H_2O$ (3)

The TFA analogue was synthesized similarly to the TCA analogue with some modifications. To synthesize this cluster, 6.64 g $Fe(NO_3)_3.9H_2O$ was added to 15 mL water and the beaker was placed on a hot plate at 150 °C. To this solution, 5.6 g $Bi(NO_3)_3.5H_2O$ was added and the mixture was boiled down to 6 mL to yield a clear red solution. This solution was then added to a 15 mL of water containing 5.5 g trifluoroacetic acid and 4.12 g sodium bicarbonate. After 2 minutes stirring, the orange white solid was separated by filtration and dissolved in 20 mL of acetone. The red needle shaped crystals formed after 3 days by slow evaporation. Elemental analysis of the crystals: Results calcd (%):C 7.82, H 1.07, F 17.62; found: C 10.07, H 1.12, F 15.89. The SQUID sample was prepared by placing the provided sample in a plastic bag, crushing the semi-crystalline sample with tweezers, rolling up the plastic bag, and placing the bag in a plastic straw that was affixed to the end of the sample rod.

Sample mass: 30.2 mg; bag mass: 9.59 mg.

Results and Discussion

The mixed addenda species {$As_4Fe_8W_{30}$} and {$Ge_2Fe_6W_{18}$}

The J_{1a} constant for the mixed addenda {$As_4Fe_8W_{30}$} system can be directly extracted using the expression $J_{1a}=(E_{BS} - E_{Smax})/30$ whereas J_{1b} for {$Ge_2Fe_6W_{18}$} can be obtained by a set of two energy differences and solving for the two unknowns J_{1b} and J' which are the inter-triad and the prismatic couplings respectively (Figures S1 and S2 in the Supplementary materials section).

These values are listed in **Table 1**. From these numbers, a noticeable trend in the motifs will be apparent as we contrast the homo-nuclear ions with the mixed addenda ones in the next section. J_{1a} (intra-triad spin coupling) has a weak magnitude generally within a dozen cm^{-1}, whereas J_{1b} (inter-triad spin coupling) is stronger. The agreement between the experimental and calculated values when existing is quite reasonable except for the $\{Ge_2Fe_6W_{18}\}$ system. The experimental value (-24 cm^{-1}) we recall originates from a single J fitting but nonetheless should lie between the real J_{1b} and J'. The calculated quantities however are nearly double the calculated value (J_{1b} = -51.8 cm^{-1} and J' = -84.3 cm^{-1}). The reason for this overestimation will be addressed when the magnetic data is estimated with these calculated values. From this comparison of the scarce set of two experimental J constants with the calculated values, only J_{1a} is quite close to that assigned from experiment differing by just 2 cm^{-1}.

Table 1 – Calculated magnetic exchange parameters obtained from the mixed addenda systems $\{Ge_2Fe_6W_{18}\}$ and $\{As_4Fe_8W_{30}\}$. Listed between parentheses are the experimental values.

Type of coupling	$\{As_4Fe_8W_{30}\}$	$\{Ge_2Fe_6W_{18}\}$
J_{1a} (cm^{-1})	-12.0 (**-14**)	-
J_{1b} (cm^{-1})	-	-51.8 (**-24**)*

*Mean value between J_{1b} and J'.

The homonuclear $\{Fe_{13}\}$ systems

Since J_{1a} and J_2 have been previously determined for **1** these values can be taken as a starting point for the present computational analysis. The J_2 value can be directly calculated from the difference $E_{BS1} - E_{Smax} = 180J_2 = -6278.5$ cm^{-1}, where **BS1** stands for the broken symmetry 'state' in which the five electrons in Fe$_{tet}$ are spin-flipped. This value can be further used to determine J_{1a} by calculating another state where the spins are flipped in one random Fe$_{oct}$ centre (**BS2**).

The energy difference will be $15J_2 + 30J_{1a}$ so that $J_2 = -34.9$ cm^{-1} and $J_{1a} = -25.8$ cm^{-1} which is in rather close agreement with the experimental values[23a] ($J_{1a} = -30$ cm^{-1}, $J_2 = -43$ cm^{-1}). However, since as many J values can be computed as there are broken symmetry states, we may surpass the two J approximation from the experimental fitting constraints and incorporate the inter-triad couplings thus introducing another exchange parameter J_{1b} associated with these. Moreover, we may improve the DFT description by calculating a selection of redundant broken symmetry states from each spin multiplicity between 5/2 and 65/2 (S_{max}) and perform a multi-variable linear regression fitting to obtain the three J values (**Table 2**). In the case of **1**, the energy values yield $J_{1a} = -5.9$ cm^{-1} $J_{1b} = -20.0$ cm^{-1} and $J_2 = -35.0$ cm^{-1}.
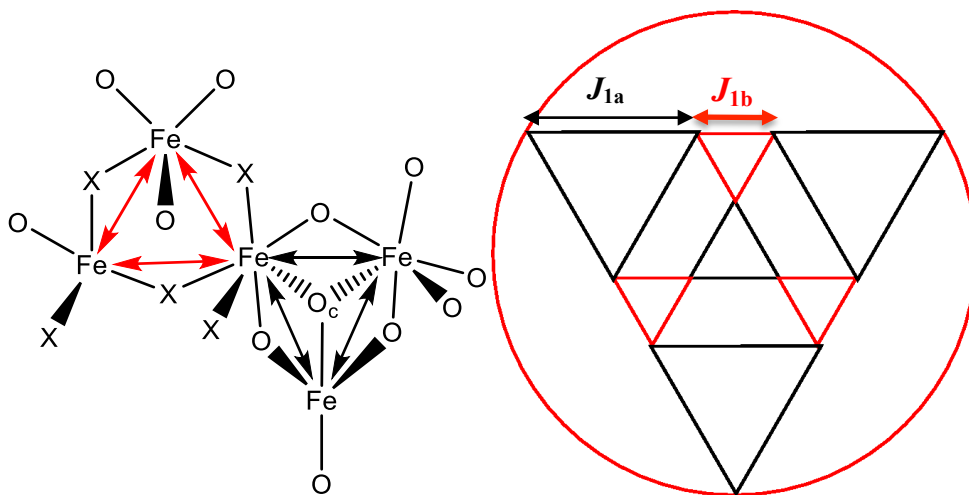
Scheme 2 - Generalized magnetic coupling pathways for the Keggin structures considered in the present DFT calculations. X denotes a bridging oxo- or fluoro- ligand.

It is evident that the two J Hamiltonian fitting does not hold. Considering ad hoc J_{1b} to be zero is clearly a wrong approximation. Also significant is the fact that the inter-triad coupling (J_{1b}) is considerably more important than the intra-triad coupling (J_{1a}). The same methodology can be equally applied to **2** and **3** such that the same values can be compared to **1**. A linear regression fit to the BS energy differences yields the values J_{1a}=-7.0 cm^{-1}, J_{1b}=-71.2 cm^{-1} and J_2=-33.2 cm^{-1}. Similarly for the newly obtained structure **3**, the values obtained are J_{1a}=-9.6, J_{1b}=-89.1 and J_2=-36.4 cm^{-1}. The linear regression fit is quite good for structures **1** and **2** as their respective R^2 values are close to unity and moderate for **3**.

While the magnitudes of J_{1a} and J_2 are similar for **1**,**2** and **3** J_{1b} is considerably higher in the latter two than for **1**. Such a change could be justified by the difference in the inter-triad bridging ligands: μ-F$^-$ in **1** versus μ-O^{2-} in **2**. Since μ-F$^-$ is more electronegative, the Fe-F bonds are more ionic in nature and therefore a smaller participation in the magnetic orbitals, generating a more difficult anti-ferromagnetic super-exchange pathway between the triads. This hypothesis is confirmed by our calculated spin densities (ϱ) of the two systems in their high spin states which reflect the extent of the spin delocalization mechanism[38] throughout the molecule: in **1** ϱ(Fe)=+4.32 ϱ(μ-F)=+0.137 whereas in **2** ϱ(Fe)=+4.23 and ϱ(μ-O)=+0.41.

The reason for the smaller value of J_{1b} in **1** with respect to **2** may also reside in the higher electronegativity of the bridging fluoride ligand that bridges the triads in **1** as posited by van Slageren and co-workers.[23a]

Table 2 - Calculated broken symmetry (BS) states of **1**, **2** and **3** and their energies relative to the highest spin state S=65/2. ΔE is defined as $E_{BS}-E_{S=65/2}$.

State	Spin	$\Delta E(1)$/cm^{-1}	$\Delta E(2)$/cm^{-1}	$\Delta E(3)$/cm^{-1}	Value
BS1	55/2	-6278.5	-6047.5	-7876.2	$180J_2$
BS2	55/2	-1296.9	-2894.4	-5166.5	$15J_2+30J_{1a}+30J_{1b}$
BS3	45/2	-6558.8	-7862.9	-10259.0	$165J_2+30J_{1a}+30J_{1b}$
BS4	35/2	-3406.2	-7969.9	-10866.8	$45J_2+90J_{1b}$
BS5	25/2	-4588.8	-9215.5	-12461.8	$60J_2+120J_{1a}+90J_{1b}$
BS6	15/2	-6734.4	-11269.3	-15456.9	$120J_2+120J_{1a}+90J_{1b}$
BS7	5/2	-5097.4	-8233.5	-10746.3	$90J_2+120J_{1a}+60J_{1b}$
J_{1a} **(cm^{-1})**		-5.9±0.3	-7.0±0.5	-9.6±4.1	
J_{1b} **(cm^{-1})**		-20.0±0.5	-71.2±0.9	-89.1±7.3	
J_2 **(cm^{-1})**		-35.0±0.3 (**-43**)	-33.2±0.5	-36.4±3.6	
RMSD from linear fit		27.8	43.4	283.7	
Adjusted R^2		1.0	1.0	0.980	

The low value of J_{1a} with respect to J_{1b} is likely related to the phenomenon of competing spin interactions where ferromagnetic polarization and AF interactions are of equal strength which is known as spin frustration, the simplest example of which is a spin triangle.[4b, 39] However not all equilateral spin triangles are spin frustrated as is evidenced by the magnitude of J_{1b}. The difference is obviously structural. Considering that the ∡Fe-X-Fe angle between and within the triads varies between 130-147° at a triad interface and 101-105° inside them. The more acute the angles are the less effective the super-exchange pathway becomes so that overall the more

prevalent AF pathways are the inter-triad pathways. This angular dependence has been characterized by Güdel et al.[40] Fe-Fe intra-triad distances are not so relevant for the magnitude of J_{1b} since in **2** they are on the order of 3.2 Å but in **3** they are close to 3.4. Inter-triad Fe-Fe distances are similar (3.3-3.5 Å).

In order to quantify the contribution that each iron $3d$ orbital plays in the anti-ferromagnetic coupling we took advantage of the Kahn-Briat formalism which states that $J_{AF} = -2t \cdot S_{ab}$, where t is the so called 'hopping integral', the gap between the in- and out-of-phase combination of the magnetic orbitals, and S_{ab} is the overlap between the interacting magnetic orbitals in magnetic centres a and b.

The unrestricted formalism we recall does not afford strictly orthogonal sets of MOs between the two spin classes. By performing a bi-orthogonalisation among two sets of alpha and beta spin orbitals, we may compute this overlap of the magnetic orbitals (S_{ab}) for the broken symmetry solution and thus evaluate the strength of the anti-ferromagnetic contribution. One way to achieve this is via the corresponding orbitals[41] approach proposed by Neese.[42] We performed a single point run[†] on the **BS2** state of structure **3**, where the spin coupling is present in all the considered sites (J_{1a}, J_{1b} and J_2), and found that $J(t_{2g}) < J(e_g^*)$. Nevertheless the $3d_\pi(t_{2g})$ orbital overlaps from the spin-flipped site are not insignificant by any means. On average, these are on the order of 0.18 for the t_{2g} set and 0.28 for the e_g^* set. There is some ligand field contribution in these valence MOs which facilitates what is called the super-exchange phenomenon in the t_{2g} set namely by the oxygen→Fe π electron donation. Since the e_g^* orbitals are anti-bonding combinations with the σ-symmetry ligand orbitals their super-exchange contribution is even larger.

Magnetic Measurements and DFT fit

From the slope of the *M* vs *H* data at 300 K, the estimation for the susceptibility of **2** is around 0.0425 cm^3/mol (cm^3 = emu/Oe) that compare relatively well with the dc data (χ_m = 0.0492 cm^3/mol at 300 K). The variable-temperature magnetic susceptibility data for **2** under an applied direct current (dc) field of 1 kOe are shown in **Figure 4**. At 300 K, the $\chi_m T$ value of 14.76 cm^3 mol^{-1} K is significantly less than the theoretical value of 56.875 cm^3 mol^{-1} K for 13 non-interacting high-spin Fe^{III} (S = 5/2, g = 2, C = 4.375 cm^3 mol^{-1} K) metal centres, indicating the presence of strong antiferromagnetic coupling. Upon lowering the temperature, the $\chi_m T$ value linearly decreases until around 50 K, then drops more sharply to 3.96 cm^3 mol^{-1} K at 2 K. The variation trend of this plot clearly demonstrates the overall appreciable antiferromagnetic coupling between the neighbouring Fe(III) centers, and, as such, this system must be frustrated, taking into account the high symmetry of the core.

The variable-temperature magnetic susceptibility data for **3** in a DC field of 1 kOe are also shown in **Figure 4**. At 300 K the $\chi_m T$ value of 13.66 emu-K mol^{-1} is significantly less than the theoretical value of 56.875 emu-K mol^{-1}, also indicating the presence of strong antiferromagnetic coupling. Upon lowering the temperature the $\chi_m T$ value decreases linearly until ~ 30 K and then drops more quickly until achieving a minimum value of 3.90 emu-K mol^{-1} at 2.0 K. This value is slightly lower than the value expected for one isolated high-spin Fe^{III} metal center (S = 5/2, g = 2, C = 4.375 emu-K mol^{-1}). The magnetic data of both compounds point to a ground state that is at least S = 5/2.
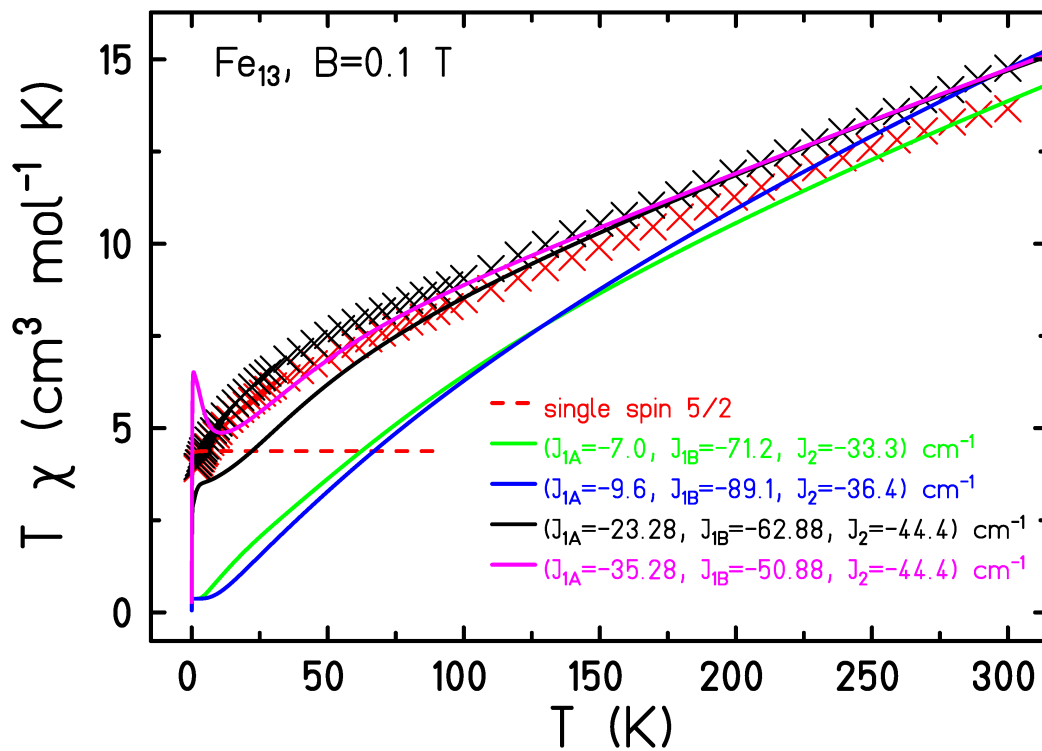
Having estimated the exchange parameters by means of DFT, spin-Hamiltonian calculations within the Heisenberg model, Eq. (2), were performed. The spectroscopic splitting factors are taken as *g=2.0*. Due to the huge dimension of the Hilbert space of

$(2S+1)^{13}=6^{13}=13{,}060{,}694{,}016$ an exact diagonalization of Hamiltonian (2) is impossible, even when considering all spin and point group symmetries.[7d, 43] But thanks to recent advances in Krylov space methods, we could evaluate magnetic observables using the Finite-Temperature Lanczos Method (FTLM).[44] This method was already successfully applied to many magnetic molecules, the largest being a cluster containing 12 Gd(III) ions with a Hilbert space dimension of 68,719,476,736 so far.[45]

The $\chi_m T$ and magnetization curves that belong to the DFT parameter sets **2** (green) and **3** (blue) in **Table 1** underestimate the experimental data. A better approximation is obtained with the values $J_2=-44.4$, $J_{1a}=-23.3$ and $J_{1b}=-62.9$ cm^{-1} (black curves), which still deviates from the experimental data points at low temperatures. A systematic fitting procedure is impossible due to the prohibitively large dimension of the Hilbert space.

It is possible that single ion anisotropy could additionally account for this deviation from the experimental curves, possibly also anisotropic exchange interactions.[17, 46] Estimations of the zero-field splitting parameters were performed† (See Supplementary Information section) and these values are significant for the octahedral iron centres ($D_{oct} \approx 1$ cm^{-1} per cation) but full diagonalisation of the anisotropic spin Hamiltonian to extract all parameters is not possible with the methodology at hand.

(a) Fe$_{13}$, B=0.1 T

single spin 5/2
(J$_{1A}$=-7.0, J$_{1B}$=-71.2, J$_2$=-33.3) cm^{-1}
(J$_{1A}$=-9.6, J$_{1B}$=-89.1, J$_2$=-36.4) cm^{-1}
(J$_{1A}$=-23.28, J$_{1B}$=-62.88, J$_2$=-44.4) cm^{-1}
(J$_{1A}$=-35.28, J$_{1B}$=-50.88, J$_2$=-44.4) cm^{-1}

(b) Fe$_{13}$, T=1.8 K

single spin 5/2
(J$_{1A}$=-7.0, J$_{1B}$=-71.2, J$_2$=-33.3) cm^{-1}
(J$_{1A}$=-9.6, J$_{1B}$=-89.1, J$_2$=-36.4) cm^{-1}
(J$_{1A}$=-23.28, J$_{1B}$=-62.88, J$_2$=-44.4) cm^{-1}
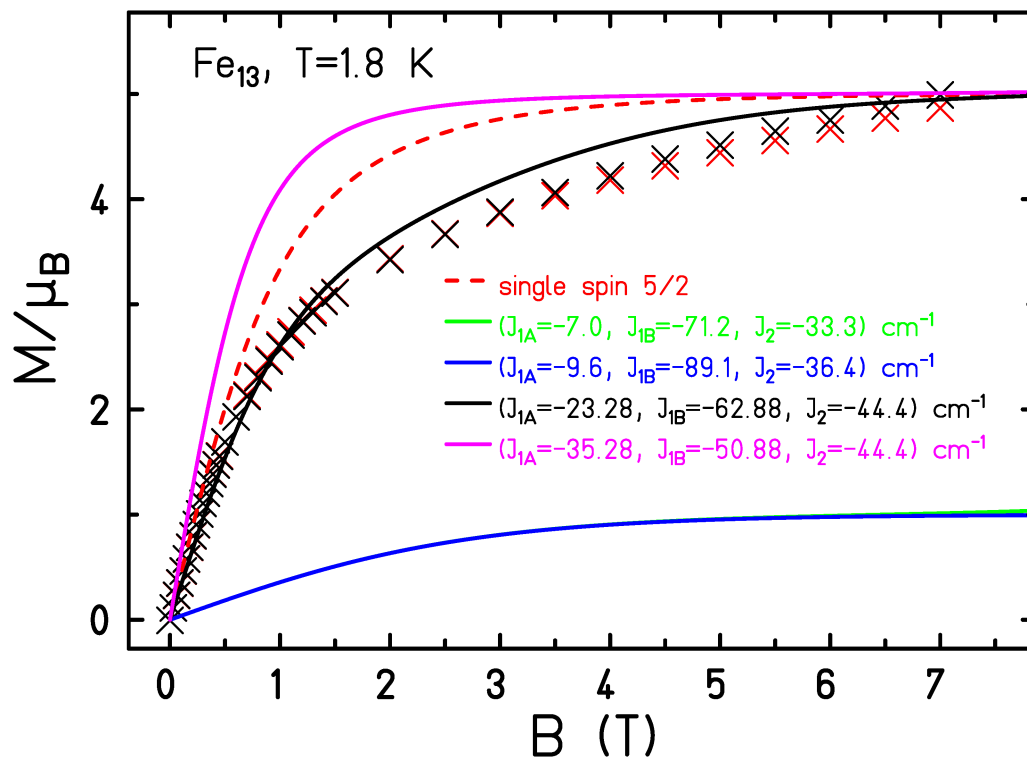(J$_{1A}$=-35.28, J$_{1B}$=-50.88, J$_2$=-44.4) cm^{-1}

Figure 4 - Susceptibility (a) and magnetization data (b) for **2** (red crosses) and **3** (dark crosses). Theoretical (FTLM) curves with different sets of J values: green and blue correspond to DFT results of **2** and **3** in Table 2, respectively. The *J* values for the black and magenta curves are guided guesses.

We attribute the inaccuracy of the DFT-based *J* values to the frustrated topology of the Keggin structure. In contrast to bipartite spin systems such as even-membered spin rings, where DFT delivers rather accurate *J* values, [14, 47] the determination of *J* values from symmetry broken states in frustrated materials seems to be delicate.[48] Take the parameter set for **2** as an example: although the broken symmetry approach might hint at a ground state spin of S=5/2, given the odd number of sites, a simple analysis yields 1/2. The reason is that J_{1b} couples the three spins 5/2 in the respective triangles to triangular ground state spins of 1/2. There are four such spins which are then aligned antiparallel to the central spin which yields a total spin of ½ in accordance with the green magnetization curve. The overestimation of J_{1b} seems to be main cause of the undervalued magnetization curve. This is consistent with the considerable B3LYP overestimation of J_{1b} with respect to its approximate experimental value as shown in **Table 1** for the $\{Ge_2Fe_6W_{18}\}$ system. However, as mentioned already, experimentally determined *J* values may also suffer from systematic errors such as unjustified approximations.

Conclusions

We performed a study of the magnetic properties of the three currently known Fe(III) homo-nuclear Keggin ions. Structural analysis indicates that in ions **2** and **3** the strongest magnetic exchange proceeds through inter-triad exchange coupling (J_{1b}) whereas only in **1** does this parameter comes second due to the nature of the bridging fluoro groups.

The shell-to-core exchange coupling (J_2) is generally invariant across the gamut of the three structures, remaining at a constant value of $\sim$ -35 cm^{-1}. The intra-triad coupling (J_{1a}) is generally the weakest in all the structures ranging between -6 and -10 cm^{-1}. From the structural motifs of the Keggin structure the anti-ferromagnetic coupling trend is generally $|J_{1b}| \quad |J_2| >$ $|J_{1a}|$.

Magnetic overlap criteria calculations indicate that the coupling between the local e_g^* set of orbitals is more efficient than the t_{2g} set of the octahedral cluster shell.

From the calculated values of **2** and **3**, a reconstruction of the magnetization and susceptibility curves was performed. The DFT exchange coupling values, when applied to the spin Hamiltonian, yield a ground state with total spin of ½ for structures **2** and **3**. The magnetization curves suggest a slightly higher spin ground state ($\sim$ 5/2) which results from the delicate balance of the three J parameters. This discrepancy with the calculated value is likely a consequence of the specific topology of the Keggin structure.

In hetero-nuclear Keggin ions the calculated J_{1a} is close to the experimental value in the $\{As_4Fe_8W_{30}\}$ structure but an over-estimation is seen for J_{1b} in the $\{Ge_2Fe_6W_{18}\}$ system which may be the root cause of the under-estimation of the magnetization curve from DFT values of both **2** and **3**.

The use of DFT methodologies in high nuclearity magnetic systems such as these is still a challenge. Although the linear fits are fairly accurate indicating consistency in the behaviour of the density functional, accurate quantitative information is still lacking in this description. The calculated parameters however do clarify the genesis of the magnetic interactions and the weight that each motif brings to the overall coupling.

The magnetic susceptibility measurements are still insufficient in number and the approximations too crude (i.e. too few number of independent J values) to allow for any extensive screening and benchmarking of the computational protocol. We hope that more extensive measurements and new crystal structures of the same family of complexes will clarify this matter.

AUTHOR INFORMATION

Corresponding Authors

 * Nuno A. G. Bandeira nbandeira@iciq.es

* Jürgen Schnack jschnack@uni-bielefeld.de

SUPPORTING INFORMATION

† Supplementary information available.

A data set collection of computational results is available in the ioChem-BD repository[49] and can be accessed via (DOI) http://dx.doi.org/10.19061/iochem-bd-1-18

REFERENCES

1. (a) Keggin, J. F. Structure of the Molecule of 12-Phosphotungstic Acid. *Nature* **1933,** *131*, 908-909; (b) Keggin, J. F. The Structure and Formula of 12-Phosphotungstic Acid. *Proc. Royal Soc. A* **1934,** *144* (851), 75-100.

2. Johansson, G. On the Crystal Structures of Some Basic Aluminium Salts. *Acta Chem. Scand.* **1960,** *14* (3), 771-773.

3. Kamb, W. B. The crystal structure of zunyite. *Acta Cryst.* **1960,** *13* (1), 15-24.

4. (a) Launay, J. P.; Verdaguer, M. *Electrons in Molecules: From Basic Principles to Molecular Electronics*. 1 ed.; OUP Oxford: 2013; p 512; (b) Kahn, O. *Molecular Magnetism*. Wiley-VCH, New York: 1993.

5. (a) Clemente-Juan, J. M.; Coronado, E.; Gaita-Arino, A. Magnetic polyoxometalates: from molecular magnetism to molecular spintronics and quantum computing. *Chem. Soc. Rev.* **2012,** *41* (22), 7464-7478; (b) Clemente-Juan, J. M.; Coronado, E.; Gaita-Ariño, A.; Suaud, N. Mixed-Valence Polyoxometalates: Spin-Coupling and Electron Distribution in the Decawolframate Anion Reduced by Two Electrons. *J. Phys. Chem. A* **2007,** *111* (39), 9969-9977; (c) Müller, A.; Peters, F.; Pope, M. T.; Gatteschi, D. Polyoxometalates: Very Large Clusters Nanoscale Magnets. *Chem. Rev.* **1998,** *98* (1), 239-272.

6. Tolis, E. I., et al. Studies of an Fe_9 Tridiminished Icosahedron. *Chem. Eur. J.* **2006,** *12* (35), 8961-8968.

7. (a) Kogerler, P.; Tsukerblat, B.; Muller, A. Structure-related frustrated magnetism of nanosized polyoxometalates: aesthetics and properties in harmony. *Dalton Trans.* **2010,** *39* (1), 21-36; (b) Kortz, U.; Müller, A.; van Slageren, J.; Schnack, J.; Dalal, N. S.; Dressel, M. Polyoxometalates: Fascinating structures, unique magnetic properties. *Coord. Chem. Rev.* **2009,** *253* (19–20), 2315-2327; (c) Müller, A., et al. Classical and Quantum Magnetism in Giant Keplerate Magnetic Molecules. *ChemPhysChem* **2001,** *2* (8-9), 517-521; (d) Schnalle, R.; Schnack, J. Numerically exact and approximate determination of energy eigenvalues for antiferromagnetic molecules using irreducible tensor operators and general point-group symmetries. *Phys. Rev. B* **2009,** *79* (10), 104419; (e) Gatteschi, D.; Sessoli, R.; Villain, J. *Molecular Nanomagnets*. OUP Oxford: 2006.

8. Dong, X.; Zhang, Y.; Liu, B.; Zhen, Y.; Hu, H.; Xue, G. Double Sandwich Polyoxometalate and Its Fe(III) Substituted Derivative, $[As_2Fe_5Mo_{21}O_{82}]^{17-}$ and $[As_2Fe_6Mo_{20}O_{80}(H_2O)_2]^{16-}$. *Inorg. Chem.* **2012,** *51* (4), 2318-2324.

9. Anderson, T. M.; Neiwert, W. A.; Hardcastle, K. I.; Hill, C. L. Multi-Iron Silicotungstates: Synthesis, Characterization, and Stability Studies of Polyoxometalate Dimers. *Inorg. Chem.* **2004,** *43* (23), 7353-7358.

10. Li, B.; Zhao, J.-W.; Zheng, S.-T.; Yang, G.-Y. A banana-shaped iron(III)-substituted tungstogermanate containing two types of lacunary polyoxometalate units. *Inorg. Chem. Commun.* **2009,** *12* (2), 69-71.

11. Zhao, J.; Han, Q.; Shi, D.; Chen, L.; Ma, P.; Wang, J.; Niu, J. Synthesis, structure and magnetism of a S-shaped multi-iron substituted arsenotungstate containing a trivacant Keggin $[B-\alpha-As^{V}W_9O_{34}]^{9-}$ and a hexavacant Keggin $[\alpha-As^{V}W_6O_{26}]^{11-}$ fragments. *J. Solid State Chem.* **2011,** *184* (10), 2756-2761.

12. Bi, L.-H.; Kortz, U.; Nellutla, S.; Stowe, A. C.; van Tol, J.; Dalal, N. S.; Keita, B.; Nadjo, L. Structure, Electrochemistry, and Magnetism of the Iron(III)-Substituted Keggin Dimer, $[Fe_6(OH)_3(A-\alpha-GeW_9O_{34}(OH)_3)_2]^{11-}$. *Inorg. Chem.* **2005,** *44* (4), 896-903.

13. Winkler, J. R.; Gray, H. B. Electronic Structures of Oxo-Metal Ions. In *Struct. Bond. : Molecular Electronic Structures of Transition Metal Complexes I* Mingos, D. M. P.; Day, P.; Dahl, J. P., Eds. Springer: 2012; Vol. 142, pp 17-28.

14. Postnikov, A. V.; Kortus, J.; Pederson, M. R. Density functional studies of molecular magnets. *Phys. Status Solidi B* **2006,** *243* (11), 2533-2572.

15. Suaud, N.; Lopez, X.; Ben Amor, N.; Bandeira, N. A. G.; de Graaf, C.; Poblet, J. M. Accuracy of Embedded Fragment Calculation for evaluating Electron Interactions in Mixed Valence Magnetic Systems: Study of 2e-reduced Lindqvist Polyoxometalates. *J. Chem. Theory Comput.* **2015,** *11* (2), 550-559.

16. (a) Tsukerblat, B.; Tarantul, A.; Müller, A. Low temperature EPR spectra of the mesoscopic cluster V15: The role of antisymmetric exchange. *J. Chem. Phys.* **2006,** *125* (5), 054714; (b) Tsukerblat, B. S.; Tarantul, A.; Müller, A. Antisymmetric exchange and pseudo Jahn–Teller instability in spin-frustrated metal clusters. *J. Mol. Struct.* **2007,** *838* (1–3), 124-132.

17.   Martens, M., et al. Anisotropy of the molecular magnet V_{15} spin Hamiltonian detected by high-field electron spin resonance. *Phys. Rev. B* **2014,** *89* (19), 195439.

18.   Bino, A.; Ardon, M.; Lee, D.; Spingler, B.; Lippard, S. J. Synthesis and Structure of $[Fe_{13}O_4F_{24}(OMe)_{12}]^{5-}$:   The First Open-Shell Keggin Ion. *J. Am. Chem. Soc.* **2002,** *124* (17), 4578-4579.

19.   Sadeghi, O.; Zakharov, L. N.; Nyman, M. Aqueous formation and manipulation of the iron-oxo Keggin ion. *Science* **2015,** *347* (6228), 1359-1362.

20.   Baumgartner, J.; Dey, A.; Bomans, P. H. H.; Le Coadou, C.; Fratzl, P.; Sommerdijk, N. A. J. M.; Faivre, D. Nucleation and growth of magnetite from solution. *Nat. Mater.* **2013,** *12* (4), 310-314.

21.   Yuwono, V. M.; Burrows, N. D.; Soltis, J. A.; Penn, R. L. Oriented aggregation: formation and transformation of mesocrystal intermediates revealed. *J. Am. Chem. Soc.* **2010,** *132* (7), 2163-2165.

22.   Pope, M. T. *Heteropoly and Isopoly Oxometalates*. Springer-Verlag: 1983.

23.   (a) Rakitin, Y. V.; van Slageren, J. Magnetic Properties of $(C_5H_6N)_5[Fe_{13}O_4F_{24}(OCH_3)_{12}] \cdot CH_3OH \cdot 4H_2O$. *Russ. J. Coord. Chem.* **2004,** *30* (11), 810-812; (b) van Slageren, J., et al. Static and dynamic magnetic properties of an $\{Fe\}_{13}$ cluster. *Phys. Rev. B* **2006,** *73* (1), 014422.

24.   Omid Sadeghi; Clément Falaise; Pedro I. Molina; Ryan Hufschmid; Charles F. Campana; Bruce C. Noll; Nigel D. Browning; Nyman, M. Chemical stabilization and electrochemical destabilization of the iron Keggin ion in water. *Inorg. Chem.* **2016,** *55* (21), 11078-11088.

25.   E.J. Baerends, et al. *Amsterdam Density Functional program*, http://www.scm.com, *Scientific Computing and Modelling* ADF-2016.01.

26.   Becke, A. D. Density-functional thermochemistry. III. The role of exact exchange. *J. Chem. Phys.* **1993,** *98*, 5648-5652.

27.   Lee, C.; Yang, W.; Parr, R. G. Development of the Colle-Salvetti correlation-energy formula into a functional of the electron density. *Phys. Rev. B* **1988,** *37*, 785-789.

28.   (a) van Lenthe, E.; Baerends, E. J.; Snijders, J. G. Relativistic regular two-component Hamiltonians. *J. Chem. Phys.* **1993,** *99*, 4597-4610; (b) van Lenthe, E.; Ehlers, A. E.; Baerends, E. J. Geometry optimizations in the zero order regular approximation for relativistic effects *J. Chem. Phys.* **1999,** *110*, 8943-8953.

29.   Van Lenthe, E.; Baerends, E. J. Optimized Slater-type basis sets for the elements 1–118. *J. Comput. Chem.* **2003,** *24* (9), 1142-1156.

30.   (a) Noodleman, L.; Norman, J. G. The X alpha valence bond theory of weak electronic coupling. Application to the low-lying states of $[Mo_2Cl_8]^{4-}$. *J. Chem. Phys.* **1979,** *70* (11), 4903-4906; (b) Noodleman, L. Valence Bond Description of Antiferromagnetic Coupling in Transition Metal Dimers. *J. Chem. Phys.* **1981,** *74* (10), 5737-5743.

31.   (a) Ruiz, E.; Rodríguez-Fortea, A.; Cano, J.; Alvarez, S.; Alemany, P. About the calculation of exchange coupling constants in polynuclear transition metal complexes. *J. Comput. Chem.* **2003,** *24* (8), 982-989; (b) Ruiz, E. Theoretical study of the exchange coupling in large polynuclear transition metal complexes using DFT methods. In *Principles and Applications of Density Functional Theory in Inorganic Chemistry II*, 1st ed.; Springer-Verlag: Berlin, 2004; Vol. 113, pp 71-102.

32.   Ruiz, E.; Alvarez, S.; Cano, J.; Polo, V. About the calculation of exchange coupling constants using density-functional theory: The role of the self-interaction error. *J. Chem. Phys.* **2005,** *123* (16), 164110.

33.   Bencini, A.; Totti, F. A Few Comments on the Application of Density Functional Theory to the Calculation of the Magnetic Structure of Oligo-Nuclear Transition Metal Clusters. *J. Chem. Theory Comput.* **2008,** *5* (1), 144-154.

34.   Klamt, A.; Schüürmann, G. COSMO: a new approach to dielectric screening in solvents with explicit expressions for the screening energy and its gradient. *J. Chem. Soc., Perkin Trans. 2* **1993,** (5), 799-805.

35.   Neese, F. The ORCA program system. *WIREs Comput. Mol. Sci.* **2012,** *2* (1), 73-78.

36.   Schafer, A.; Horn, H.; Ahlrichs, R. Fully optimized contracted Gaussian basis sets for atoms Li to Kr. *J. Chem. Phys.* **1992,** *97* (4), 2571-2577.

37.   (a) Kossmann, S.; Neese, F. Comparison of two efficient approximate Hartee–Fock approaches. *Chem. Phys. Lett.* **2009,** *481* (4-6), 240-243; (b) Neese, F.; Wennmohs, F.; Hansen, A.; Becker, U. Efficient, approximate and parallel Hartree–Fock and hybrid DFT calculations. A 'chain-of-spheres' algorithm for the Hartree–Fock exchange. *Chem. Phys.* **2009,** *356* (1-3), 98-109.

38.   Cano, J.; Ruiz, E.; Alvarez, S.; Verdaguer, M. Spin Density Distribution in Transition Metal Complexes: Some Thoughts and Hints. *Comments Inorg. Chem.* **1998,** *20* (1), 27 - 56.

39.   (a) Schnack, J. Effects of frustration on magnetic molecules: a survey from Olivier Kahn until today. *Dalton Trans.* **2010,** *39* (20), 4677-4686; (b) Verdaguer, M.; Robert, V. 8.04 - Fundamentals, Principles, and Concepts of Molecular Magnetism and Spintronics In *Comprehensive Inorganic Chemistry II (Second Edition)*, Poeppelmeier, K., Ed. Elsevier: Amsterdam, 2013; Vol. 8, pp 131-189.

40.   Weihe, H.; Güdel, H. U. Angular and Distance Dependence of the Magnetic Properties of Oxo-Bridged Iron(III) Dimers. *J. Am. Chem. Soc.* **1997,** *119* (28), 6539-6543.

41.   Amos, A. T.; Hall, G. G. Single Determinant Wave Functions. *Proc. Roy. Soc. (London) Ser. A* **1961,** *263* (1315), 483-493.

42.   Neese, F. Definition of corresponding orbitals and the diradical character in broken symmetry DFT calculations on spin coupled systems. *J. Phys. Chem. Solids* **2004,** *65* (4), 781-785.

43.   (a) Waldmann, O. Symmetry and energy spectrum of high-nuclearity spin clusters. *Phys. Rev. B* **2000,** *61* (9), 6138-6144; (b) Schnalle, R.; Schnack, J. Calculating the energy spectra of magnetic molecules: application of real- and spin-space symmetries. *Int. Rev. Phys. Chem.* **2010,** *29* (3), 403-452.

44.   (a) Jaklič, J.; Prelovšek, P. Lanczos method for the calculation of finite-temperature quantities in correlated systems. *Physical Review B* **1994,** *49* (7), 5065-5068; (b) Schnack, J.; Wendland, O. Properties of highly frustrated magnetic molecules studied by the finite-temperature Lanczos method. *Eur. Phys. J. B* **2010,** *78* (4), 535-541; (c) Schnack, J.; Heesing, C. Application of the finite-temperature Lanczos method for the evaluation of magnetocaloric properties of large magnetic molecules*. *Eur. Phys. J. B* **2013,** *86* (2), 46.

45.   Zheng, Y.; Zhang, Q.-C.; Long, L.-S.; Huang, R.-B.; Muller, A.; Schnack, J.; Zheng, L.-S.; Zheng, Z. Molybdate templated assembly of Ln12Mo4-type clusters (Ln = Sm, Eu, Gd) containing a truncated tetrahedron core. *Chem. Commun.* **2013,** *49* (1), 36-38.

46.   Pineda, E. M.; Lorusso, G.; Zangana, K. H.; Palacios, E.; Schnack, J.; Evangelisti, M.; Winpenny, R. E. P.; McInnes, E. J. L. Observation of the influence of dipolar and spin frustration effects on the magnetocaloric properties of a trigonal prismatic {Gd7} molecular nanomagnet. *Chem. Sci.* **2016,** *7* (8), 4891-4895.

47.   Postnikov, A. V.; Chiuzbăian, S. G.; Neumann, M.; Blügel, S. Electron spectroscopy and density-functional study of 'ferric wheel' molecules. *J. Phys. Chem. Solids* **2004,** *65* (4), 813-817.

48.   Hanebaum, O.; Schnack, J. Thermodynamic observables of {Mn}12-acetate calculated for the full spin Hamiltonian. *Phys. Rev. B* **2015,** *92* (6), 064424.

49.   Álvarez-Moreno, M.; de Graaf, C.; López, N.; Maseras, F.; Poblet, J. M.; Bo, C. Managing the Computational Chemistry Big Data Problem: The ioChem-BD Platform. *J. Chem. Inf. Model.* **2015,** *55* (1), 95-103.

SYNOPSIS TOC

The family of Fe[III] homonuclear Keggin structures is studied computationally to probe into their magnetic properties and the exchange parameters are used to reconstruct the experimental magnetization curves. The (edge-sharing) triads afford the lowest *J* value whereas the tip-sharing inter-triad borders are the most favorable anti-ferromagnetic pathway in contrast to what had been previously assumed.

J_{1a} J_{1b}